Molecular dynamics analysis of incoherent neutron scattering from light water via the Van Hove space–time self-correlation function with a new quantum correction

Y. Abe *, S. Tasaki

Department of Nuclear Engineering, Kyoto University, Kyotodaigaku-Katsura, Nishikyo-ku, Kyoto 615-8540, Japan

ABSTRACT

In this paper, we propose a general method for evaluating the neutron incoherent scattering cross-section of light water by molecular dynamics (MD) analysis of the Van Hove space–time self-correlation function (STSCF) with a newly developed quantum correction named as Gaussian approximation-assisted quantum correction (GAAQC). The self-intermediate scattering function (SISF) by GAAQC satisfies the detailed balance condition and sum rules up to second order adequately, and approaches for long times the one obtained directly from MD trajectory data. These features are desirable for the evaluation of the neutron scattering cross-section over a wide range of energy and momentum transfer. From the analysis of quasi-elastic scattering, the self-scattering law by GAAQC shows the jump-diffusive behavior of the molecular translational motion, which is not reproduced by Gaussian approximation (GA). As compared with GA, double differential and total cross-sections by GAAQC show better agreement with experimental data, particularly below the cold neutron region where the non-Gaussian property of the SISF becomes apparent. Thus, the present method, namely, the direct analysis of the STSCF with GAAQC will serve for improving the evaluation of the neutron scattering cross-section for light water.

© 2015 Elsevier Ltd. All rights reserved.

1. Introduction

Neutron scattering cross-section data of light water have been extensively utilized for the design and analysis of reactor cores and cold neutron sources. In recent years, they are also referred for the analysis of neutron imaging data from various water-containing materials (Biesdorf et al., 2014; Kiyanagi et al., 2012; Josic et al., 2012; Muhrer et al., 2012; Kawabata et al., 2005). Owing to large incoherent scattering from hydrogen, cold and thermal neutron scattering cross-sections for these materials are dominated by the motion of hydrogen. Thus, any variations of the total neutron cross-section from bulk water, which could be measured by neutron time-of-flight (TOF) imaging (Kardjilov et al., 2003; Kiyanagi et al., 2005), may provide information on the dynamical state of water. Such use of the neutron imaging may bring a new possibility of the nondestructive inspection for water-containing materials. However, dynamical information, which appears principally in the double differential cross-section, tends to be featureless in the total cross-section. Thus, for the better

identification and understanding of the dynamical state of water from the variation of the total cross-section, theoretical analysis of the total cross-section for water would also be necessary as a complementary approach.

According to the Van Hove theory (Van Hove, 1954), the thermal neutron scattering cross-section is represented as the Fourier transformation of the space–time correlation function (STCF) of the particle-density operator for the target system. But in general, because of the many-body problem, determining the exact form of the STCF is difficult. Hence, the existing thermal neutron scattering libraries for various materials (Chadwick, 2006; Mattes and Keinert, 2005) have been evaluated on the basis of physical models, which inevitably involve errors coming from assumptions of the models, and difficulties in determining the value of model parameters over a wide range of temperatures. Therefore, in the previous study (Abe et al., 2014), we applied molecular dynamics (MD) to the analysis of the neutron scattering cross-section for light water for the purpose of improving the evaluation method, and found better agreement with experiments on the total cross-section for cold neutrons in comparison with ENDF/B-VII (Chadwick, 2006). Around the same time, similar results were reported independently by the group at the Bariloche Atomic Centre (Marquez Damian et al., 2013;

Márquez Damián et al., 2014), and their results also confirmed the effectiveness of the MD-based evaluation.

In both the existing nuclear data libraries and MD-based evaluations mentioned above, Gaussian approximation (GA) is utilized in representing the self-intermediate scattering function (SISF), which is defined as the Fourier transformation in space of the space–time self-correlation function (STSCF). The grounds for GA are based on the fact that the SISF is exactly represented by the Gaussian function of the scattering vector κ for recoil scattering from free atoms at large κ and for quasi-elastic neutron scattering (QENS) from diffusing atoms at small κ. On GA, the width function, which gives the standard deviation of the Gaussian function, is formulated by the frequency distribution function for the target system, allowing the SISF to satisfy the detailed balance condition and sum rules up to second order (Rahman et al., 1962). These properties of the SISF by GA are desirable for applying over a wide region in the κ–t plane, and the calculation of the scattering cross-section by GA is relatively straightforward once the frequency distribution for the target system is given by physical models or MD simulations. Thus, GA has been used for the evaluation of thermal neutron scattering cross-sections.

However, the SISF is not assured to be Gaussian for all ranges of κ. Moreover, as hydrogen bonds among water molecules are relatively strong, the diffusion of water cannot be explained by the continuous diffusion model, but by the jump-diffusion model (Singwi and Sjölander, 1960). In the jump-diffusion model several water molecules are assumed to form a transient network, oscillating around their residence sites between successive jumps which is caused by the collapse of the network due to the molecular thermal motion. Such jump-diffusional motion of water was observed by QENS (Teixeira et al., 1985), where the half width at half maximum (HWHM) of QENS peaks showed suppression from the linear relationship with κ^2 (In case of the continuous diffusion, the HWHM of QENS peaks is proportional to κ^2). The SISF represented by the jump-diffusion model contains a decay constant of the network and becomes a non-Gaussian function of κ. This non-Gaussian behavior of the SISF may influence on the neutron scattering cross-section below cold neutron energies where QENS is significant. Therefore, in order to consider the non-Gaussian property of the SISF adequately, the neutron scattering cross-section for light water should be analyzed directory from the Van Hove STSCF by statistical processing of MD trajectory data.

But there is an essential problem that the STSCF from MD simulations cannot be identified with the one in the Van Hove theory. This is because MD simulation is based on classical mechanics while the Van Hove theory on quantum mechanics. As a result, the SISF from MD simulations do not reproduce quantum effects such as the detailed balance condition and sum rules, and hence must be corrected to satisfy them for the evaluation of neutron scattering cross-sections. Although several quantum corrections (QCs) have been developed in order to recover the detailed balance condition (Schofield, 1960; Egelstaff, 1962; Aamodt et al., 1962), to our knowledge, none of them satisfy high-order sum rules simultaneously. Sum rules up to second order are particularly important for the evaluation of deep inelastic neutron scattering above several eV because the peak position and width of recoil scattering depend on the first and second moments of the self-scattering law.

Thus, the purposes of the present study are to develop a new QC which satisfies both the detailed balance condition and high-order sum rules adequately, and to examine the effectiveness of the direct analysis of the STSCF with the new QC by comparing with the previous results based on GA. The present paper is organized as follows. Chapter 2 describes the method for the evaluation of the neutron scattering cross-section by MD and proposes a new QC. In Chapter 3, calculated results are shown and discussed as compared with GA and conventional QCs. Finally in Chapter 4, a few concluding remarks are mentioned.

2. The method for the evaluation of the scattering cross-section

2.1. The framework of the present method

Owing to the large incoherent scattering cross-section of hydrogen, the double differential scattering cross-section per molecule can be represented by the incoherent approximation:

$$\frac{\mathrm{d}^2\sigma_s}{\mathrm{d}\Omega\mathrm{d}\varepsilon} = \frac{2}{\hbar}\frac{\sigma_b^H}{4\pi}\sqrt{\frac{E}{E_0}}S_s^H(\kappa,\omega) + \frac{1}{\hbar}\frac{\sigma_b^O}{4\pi}\sqrt{\frac{E}{E_0}}S_s^O(\kappa,\omega), \tag{1}$$

where $\hbar$ is the Planck constant divided by 2π, σ_b^H and σ_b^O are the bound-atom cross-sections for hydrogen and oxygen, $S_s^H(\kappa,\omega)$ and $S_s^O(\kappa,\omega)$ are self-scattering laws for hydrogen and oxygen, and E_0 and E are the energies of the incident and scattered neutrons. The energy and momentum transfers of neutrons are defined as $\hbar\omega = E_0 - E$ and $\hbar\kappa = \hbar|\boldsymbol{k}_0 - \boldsymbol{k}|$. Here, $\boldsymbol{k}_0$ and $\boldsymbol{k}$ are the wave vectors of the incident and scattered neutrons. The self-scattering law is defined by

$$S_s^X(\kappa,\omega) = \frac{1}{2\pi}\int_{-\infty}^{\infty}\mathrm{d}te^{-i\omega t}F_s^X(\kappa,t), \tag{2}$$

where $F_s^X(\kappa,t)$ is the SISF. Note that X denotes hydrogen by X = H or oxygen by X = O.

Instead of GA used in the previous study (Abe et al., 2014), we return to the STSCF $G_s^X(r,t)$ for the evaluation of $F_s^X(\kappa,t)$, where $F_s^X(\kappa,t)$ is defined as the Fourier transformation of $G_s^X(r,t)$ in space $\boldsymbol{r}$:

$$F_s^X(\kappa,t) = \int \mathrm{d}\boldsymbol{r}\, e^{i\boldsymbol{\kappa}\cdot\boldsymbol{r}}\, G_s^X(r,t). \tag{3}$$

Based on classical mechanics, $G_s^X(r,t)\mathrm{d}\boldsymbol{r}$ means the probability of finding a X-atom in the thin shell $\mathrm{d}\boldsymbol{r}(= 4\pi r^2\mathrm{d}r)$ at a distance r from the origin at time t, provided the same atom exists at the origin at $t = 0$. Therefore, the classical STSCF $\widetilde{G}_s^X(r,t)$ can be calculated from MD trajectory data as below:

$$\widetilde{G}_s^X(r,t) = \langle\delta\left(\boldsymbol{r} - \boldsymbol{R}_i^X(t+\tau) + \boldsymbol{R}_i^X(\tau)\right)\rangle_c, \tag{4}$$

where $\boldsymbol{R}_i^X(\tau)$ is the position of the i-th X-atom at time τ and the notation $\langle\ldots\rangle_c$ denotes the average over time τ and atoms i with keeping the lag-time t constant. Note that the target system is assumed to be isotropic, thus in the left-hand side of Eq. (4) the vector $\boldsymbol{r}$ is reduced to the scalar r. As $G_s^X(r,t)$ in Eq. (3) cannot be identified with the classical one $\widetilde{G}_s^X(r,t)$ in Eq. (4), a QC of $\widetilde{G}_s^X(r,t)$ must be carried out for the reconstruction of the scattering cross-section through Eqs. (1)–(3). This will be discussed in the next subsection.

2.2. The quantum correction for the SISF

We begin with the QC of the classical SISF $\widetilde{F}_s^X(\kappa,t)$ proposed by Sears (1985), which was intended to fulfill sum rules higher than first order for almost-classical liquid systems. In this correction, $F_s^X(\kappa,t)$ is represented by

$$F_s^X(\kappa,t) = R(\kappa,t)\widetilde{F}_s^X(\kappa,t), \tag{5}$$

where $R(\kappa,t)$ is a correction function. From Eq. (2), $S_s^X(\kappa,\omega)$ is represented by the convolution integral between $Q(\kappa,\omega)$ and $\widetilde{S}_s^X(\kappa,\omega)$ if we define $Q(\kappa,\omega)$ and $\widetilde{S}_s^X(\kappa,\omega)$ as the Fourier transformations of

$R(\kappa, t)$ and $\widetilde{F}_s^X(\kappa, t)$ in time t, respectively. Assuming that the target system is almost classical, $Q(\kappa, \omega)$ can be approximately considered as a delta function $\delta(\omega)$ because $R(\kappa, t) \simeq 1$. Thus, by expanding $\widetilde{S}_s^X(\kappa, \omega)$ in Taylor series around the point where $Q(\kappa, \omega)$ have a significant value, $S_s^X(\kappa, \omega)$ may be written in a convergent expansion series. Summing up the series, $S_s^X(\kappa, \omega)$ can formally satisfy high-order sum rules.

However, the assumption of the classical approximation is satisfied for long times $t \gg t_{cls}$, where t_{cls} is the characteristic time of the classical approximation defined by $t_{cls} = 2\pi\hbar/(k_B T)$ with the Boltzmann constant k_B and temperature T. This corresponds to $t_{cls} \simeq 0.16$ ps at $T = 300$ K. On the other hand, for deep inelastic scattering where the energy transfer of incident neutrons ε amounts to about 1 eV, the above assumption is not fulfilled because the collision time $t_{col} = 2\pi\hbar/\varepsilon \simeq 4.1$ fs is much smaller than t_{cls}. Thus, for high incident energies, Sears's QC cannot be applicable to the evaluation of the scattering cross-section in its original form.

Viewing Eq. (5) from different angles, the correction function $R(\kappa, t)$ can be estimated if a pair of quantum and classical SISFs are found. In the present study, we choose the SISFs by GA as this pair. Therefore, the newly developed QC is represented as follows:

$$F_s^X(\kappa, t) = \frac{F_s^{X,G}(\kappa, t)}{\widetilde{F}_s^{X,G}(\kappa, t)} \widetilde{F}_s^X(\kappa, t), \tag{6}$$

where $F_s^{X,G}(\kappa, t)$ is the SISF by GA and $\widetilde{F}_s^{X,G}(\kappa, t)$ is the classical limit ($\hbar \to 0$) of $F_s^{X,G}(\kappa, t)$. The functions $F_s^{X,G}(\kappa, t)$ and $\widetilde{F}_s^{X,G}(\kappa, t)$ are given by Rahman et al. (1962)

$$F_s^{X,G}(\kappa, t) = \exp\left[-\frac{\kappa^2}{2}\Gamma^X(t)\right] \tag{7}$$

and

$$\widetilde{F}_s^{X,G}(\kappa, t) = \exp\left[-\frac{\kappa^2}{2}\tilde{\Gamma}^X(t)\right] \tag{8}$$

with

$$\Gamma^X(t) = \frac{\hbar}{m_X}\int_0^\infty d\omega \frac{g^X(\omega)}{\omega}\left\{\coth\left(\frac{\hbar\omega\beta}{2}\right)(1 - \cos\omega t) - i\sin\omega t\right\} \tag{9}$$

and

$$\tilde{\Gamma}^X(t) = \frac{2}{m_X\beta}\int_0^\infty d\omega \frac{g^X(\omega)}{\omega^2}(1 - \cos\omega t), \tag{10}$$

where $\Gamma^X(t)$ and $\tilde{\Gamma}^X(t)$ are, respectively, the width functions for $F_s^{X,G}(\kappa, t)$ and $\widetilde{F}_s^{X,G}(\kappa, t)$, m_X is the mass of a X-atom and $\beta = 1/(k_B T)$. The function $g^X(\omega)$ is the generalized frequency function defined by

$$g^X(\omega) = \frac{2m_X\beta}{3\pi}\int_0^\infty dt \langle \boldsymbol{v}^X(\tau) \cdot \boldsymbol{v}^X(t + \tau)\rangle_c \cos\omega t, \tag{11}$$

where $\langle \boldsymbol{v}^X(\tau) \cdot \boldsymbol{v}^X(t + \tau)\rangle_c$ is the velocity auto-correlation function (VACF) for X. The integral of $g^X(\omega)$ over positive ω is normalized to unity (Abe et al., 2014). Hereafter, we call the present correction as Gaussian approximation-assisted quantum correction (GAAQC). Note that $F_s^X(\kappa, t)$ by GAAQC satisfies the relation $F_s^X(\kappa, t) = \left(F_s^X(\kappa, -t)\right)^*$, which is necessary to make $S_s^X(\kappa, \omega)$ real. In the next, the other properties of GAAQC such as the short and long time behaviors, the detailed balance condition and sum rules are examined.

2.3. The properties of GAAQC

2.3.1. The short time limit

In the short time limit, atoms in the MD simulation can be considered to move freely. Therefore, the SISF directly calculated from MD $\widetilde{F}_s^X(\kappa, t)$ approaches the one of free gas in the classical approximation:

$$\widetilde{F}_s^X(\kappa, t) \simeq \exp\left[-\frac{\kappa^2}{2}\frac{t^2}{m_X\beta}\right]. \tag{12}$$

From Eqs. (8) and (10), $\widetilde{F}_s^{X,G}(\kappa, t)$ also approaches the same SISF as Eq. (12) for $t \to 0$. Thus, in the short time limit, we can approximate Eq. (6) as

$$F_s^X(\kappa, t) \simeq F_s^{X,G}(\kappa, t). \tag{13}$$

Moreover, from Eqs. (7) and (9), the short time behavior of $F_s^{X,G}(\kappa, t)$ is found to be free gas as well:

$$F_s^{X,G}(\kappa, t) \simeq \exp\left[-\frac{\kappa^2}{2}\left(\frac{t^2}{m_X\beta_{eff}^X} - i\frac{\hbar t}{m_X}\right)\right], \tag{14}$$

where $\beta_{eff}^X = 1/(k_B T_{eff}^X)$ with the effective temperature T_{eff}^X defined by

$$T_{eff}^X = T\int_0^\infty d\omega\, g^X(\omega)\frac{\hbar\omega\beta}{2}\coth\left(\frac{\hbar\omega\beta}{2}\right). \tag{15}$$

Note that the effective temperature T_{eff}^X differs from the liquid temperature T because it involves the zero-point energy for the intra-molecular vibrations of hydrogen and oxygen through $g^X(\omega)$. From Eq. (15), T_{eff}^X gets close to T toward high temperatures ($\beta \to 0$) since the zero-point energy is negligible as compared with the thermal energy. As a quantum effect, $F_s^{X,G}(\kappa, t)$ in Eq. (14) contains an imaginary term which gives the recoil energy $E_r^X = \hbar^2\kappa^2/(2m_X)$, while the classical SISF in Eq. (12) lacks this term.

2.3.2. The long time limit

The long time behavior of $F_s^X(\kappa, t)$ is evaluated using the definitions of the delta function $\delta(\omega)$:

$$\delta(\omega) = \lim_{t\to\infty}\frac{\sin\omega t}{\pi\omega} = \lim_{t\to\infty}\frac{\sin^2\omega t}{\pi\omega^2 t}. \tag{16}$$

Using Eq. (16) in Eqs. (9) and (10), and defining the diffusion coefficient D^X for X by $D^X = \pi g^X(0)/(2m_X\beta)$, the asymptotic forms of $F_s^{X,G}(\kappa, t)$ and $\widetilde{F}_s^{X,G}(\kappa, t)$ in the long time limit are evaluated as follows:

$$F_s^{X,G}(\kappa, t) \simeq \exp\left[-D^X\kappa^2\left(t - i\frac{\hbar\beta}{2}\right)\right] \simeq \exp\left[-D^X\kappa^2 t\right] \tag{17}$$

and

$$\widetilde{F}_s^{X,G}(\kappa, t) \simeq \exp\left[-D^X\kappa^2 t\right]. \tag{18}$$

In the last line of Eq. (17), the relation $t \gg \hbar\beta/2$ is assumed. From above equations, both $F_s^{X,G}(\kappa, t)$ and $\widetilde{F}_s^{X,G}(\kappa, t)$ coincide asymptotically with the SISF for the continuous diffusion. Thus, at the long time, we can approximate Eq. (6) as

$$F_s^X(\kappa, t) \simeq \widetilde{F}_s^X(\kappa, t). \tag{19}$$

This indicates that the non-Gaussian behavior of the SISF for light water can be involved in $F_s^X(\kappa, t)$ since $\widetilde{F}_s^X(\kappa, t)$ is directly calculated from MD trajectory data.

2.3.3. The detailed balance condition

Next, we will examine whether $F_s^X(\kappa, t)$ by GAAQC fulfills the detailed balance condition. For an isotropic system, the detailed balance condition for $F_s^X(\kappa, t)$ is represented as follows:

$$F_s^X(\kappa, -t + i\hbar\beta) = F_s^X(\kappa, t). \tag{20}$$

From Eq. (6), the left-hand side of Eq. (20) is rewritten as

$$
\begin{aligned}
F_s^X(\kappa, -t + i\hbar\beta) &= \frac{F_s^{X,G}(\kappa, -t + i\hbar\beta)}{\widetilde{F}_s^{X,G}(\kappa, -t + i\hbar\beta)} \widetilde{F}_s^X(\kappa, -t + i\hbar\beta) \\
&= F_s^{X,G}(\kappa, t) \frac{\widetilde{F}_s^X(\kappa, -t + i\hbar\beta)}{\widetilde{F}_s^{X,G}(\kappa, -t + i\hbar\beta)}.
\end{aligned} \tag{21}
$$

In the last line of Eq. (21), we use the property of $F_s^{X,G}(\kappa, t)$, that is, $F_s^{X,G}(\kappa, -t + i\hbar\beta) = F_s^{X,G}(\kappa, t)$ (Rahman et al., 1962). At the short time ($t \ll \hbar\beta$), using Eq. (21) with the relations $F_s^{X,G}(\kappa, t) \simeq F_s^X(\kappa, t)$ and $\widetilde{F}_s^X(\kappa, t) \simeq \widetilde{F}_s^{X,G}(\kappa, t)$, we have $F_s^X(\kappa, -t + i\hbar\beta) = F_s^X(\kappa, t)$. Thus, $F_s^X(\kappa, t)$ is assured to satisfy the detailed balance condition of Eq. (20). At the long time ($t \gg \hbar\beta$), the imaginary time $i\hbar\beta$ in Eq. (21) can be negligible. Thus, $F_s^X(\kappa, t)$ satisfies the detailed balance condition of Eq. (20) again since $\widetilde{F}_s^X(\kappa, t)$ and $\widetilde{F}_s^{X,G}(\kappa, t)$ are even functions of t. As shown above, $F_s^X(\kappa, t)$ by GAAQC satisfies the detailed balance condition at short and long times. Hence, $F_s^X(\kappa, t)$ is reasonably supposed to satisfy it approximately for intermediate times as well.

2.3.4. Sum rules

At the end of this section, we examine sum rules for $S_s^X(\kappa, \omega)$ by GAAQC. The n-th moment $S_n^X(\kappa)$ of $S_s^X(\kappa, \omega)$ can be calculated by using the following relation:

$$S_n^X(\kappa) = \int_{-\infty}^{\infty} S_s^X(\kappa, \omega)(\hbar\omega)^n d\omega = \left(\frac{\hbar}{i}\right)^n \frac{\partial^n}{\partial t^n} F_s^X(\kappa, t)\Big|_{t=0}. \tag{22}$$

From Eqs. (14) and (22), the first three moments are obtained as follows:

$$S_0^X(\kappa) = 1, \; S_1^X(\kappa) = E_r^X \; \text{and} \; S_2^X(\kappa) = \left(E_r^X\right)^2 + \frac{4}{3} E_r^X \overline{K}^X, \tag{23}$$

where $\overline{K}^X$ is the mean kinetic energy for X defined by $\overline{K}^X = 3k_B T_{eff}^X / 2$. Therefore, $S_s^X(\kappa, \omega)$ by GAAQC is confirmed to fulfill sum rules up to second order.

3. Results and discussions

3.1. The MD simulation and the analysis of the STSCF

The MD simulation of light water is carried out under the condition of constant volume and temperature (NVT ensemble) using the SPC potential model with intra-molecular vibrations (Dang and Pettitt, 1987). To examine the non-Gaussian behavior of the SISF for light water, two temperatures 293.6 and 350 K are selected from the previous study (Abe et al., 2014). The simulation conditions are listed in Table 1. As a MD simulation code, DL_POLY

Table 1
The simulation conditions.

Run no.	#1	#2
Temperature (K)	293.6	350
Density (g/cm³)	1.0	0.97
Time step interval (fs)	0.1	0.1
Number of time steps	10^6	10^6
Number of molecules	216	216

(Smith et al., 2002) is used. The position and velocity vectors of 216 molecules are calculated in the cubic simulation system with the periodic boundary condition. Trajectory data of all the atoms are stored in a file at every time step, and then utilized for the analysis of the STSCF and VACF. The evaluation procedure for the VACF and width functions is the same as the previous study. Except for MD simulations by DL_POLY, our originally developed codes are used for all the calculations hereafter.

On the calculation of $\widetilde{G}_s^X(r, t)$, the radial range from 0 to 15 Å is divided into 10^4 bins and the lag-time t is sampled from 0 to 10 ps with an interval Δt of 1 fs. With keeping the lag-time t constant, $\widetilde{G}_s^X(r, t)$ is evaluated by counting the number of X-atoms within each radial bin, and then, according to Eq. (3), $\widetilde{F}_s^X(\kappa, t)$ is calculated by the Fourier transformation of $\widetilde{G}_s^X(r, t)$ in space r. The maximum of the radial range $r_{max} = 15$ Å is chosen to be smaller than the dimension of the simulation system so as not to cause artifacts due to the periodic boundary condition. The number of radial bins $N_r = 10^4$ determines the maximum of the wave number transfer κ_{max} by $\kappa_{max} = \pi N_r / r_{max}$ due to the sampling theorem. In order to evaluate the molecular motions in the short time adequately, $N_r = 10^4$ is chosen so as to make the width of the radial bin Δr much less than the migration length ΔL of hydrogen atoms within Δt. In the present study, this can be assured because $\Delta r = 1.5 \times 10^{-3}$ Å is sufficiently small as compared with $\Delta L \simeq 2 \times 10^{-2}$ Å. The maximum lag-time and the number of sampling points are selected mainly by our available computing resources. The maximum lag-time $t_{max} = 10$ ps in the present calculation may be barely sufficient to evaluate the diffusive motion of water molecules around normal temperatures. Thus, the accessible region of $\widetilde{F}_s^X(\kappa, t)$ in the κ-t plane is limited by κ_{max} and t_{max}, and beyond them, the following extrapolations

$$
\widetilde{F}_s^X(\kappa, t) = \begin{cases}
\frac{\widetilde{F}_s^X(\kappa, t_{max})}{\widetilde{F}_s^{X,G}(\kappa, t_{max})} \widetilde{F}_s^{X,G}(\kappa, t) & (\kappa \leqslant \kappa_{max}, \; t > t_{max}) \\[2mm]
\frac{\widetilde{F}_s^X(\kappa_{max}, t)}{\widetilde{F}_s^{X,G}(\kappa_{max}, t)} \widetilde{F}_s^{X,G}(\kappa, t) & (\kappa > \kappa_{max}, \; t \leqslant t_{max}) \\[2mm]
\frac{\widetilde{F}_s^X(\kappa_{max}, t_{max})}{\widetilde{F}_s^{X,G}(\kappa_{max}, t_{max})} \widetilde{F}_s^{X,G}(\kappa, t) & (\kappa > \kappa_{max}, \; t > t_{max})
\end{cases} \tag{24}
$$

are made on the evaluation of the scattering cross-section. Note that $\widetilde{F}_s^{X,G}(\kappa, t)$ can be evaluated over all regions in the κ-t plane since $\widetilde{F}_s^{X,G}(\kappa, t)$ is represented by the Gaussian function of κ and the asymptotic form of $\widetilde{F}_s^{X,G}(\kappa, t)$ at the long time can be approximated by Eq. (18).

3.2. The short and long time behaviors of GAAQC

Three SISFs for hydrogen are calculated at $\kappa = 1.6$ Å^{-1} and $T = 293.6$ K by GA ($F_s^{H,G}(\kappa, t)$), by the direct calculation with GAAQC ($F_s^H(\kappa, t)$) and by the direct calculation with no QC ($\widetilde{F}_s^H(\kappa, t)$). The absolute values of the SISFs and the quantum correction factor $R(\kappa, t) = F_s^{H,G}(\kappa, t)/\widetilde{F}_s^{H,G}(\kappa, t)$ are shown in Fig. 1. At the short time, $F_s^H(\kappa, t)$ almost coincides with $F_s^{H,G}(\kappa, t)$ as shown in Eq. (13). Increasing the lag-time, the crossover of $F_s^H(\kappa, t)$ from $F_s^{H,G}(\kappa, t)$ to $\widetilde{F}_s^H(\kappa, t)$ around $t_{cls} \simeq 0.16$ ps is obvious. Above several ps, $F_s^H(\kappa, t)$ approaches $\widetilde{F}_s^H(\kappa, t)$, which is predicted by Eq. (19) as an asymptotic property of GAAQC. Likewise, the absolute value of $R(\kappa, t)$ shows a rapid decrease from unity in the small time region ($t < 0.1$ ps) where the quantum effect is significant, while it becomes constant for long times ($t > 1$ ps) where the target system is considered to be classical. Therefore, the expected properties of the SISF by GAAQC are confirmed.
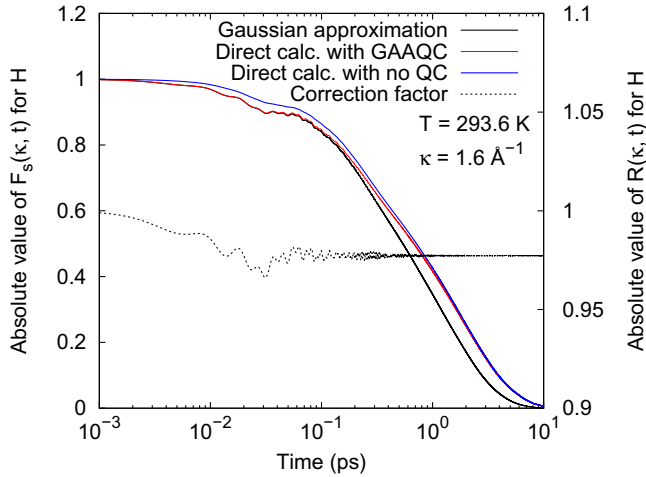
Fig. 1. The absolute value of the SISFs (left axis) and the quantum correction factor (right axis) for hydrogen at $T = 293.6$ K and $\kappa = 1.6$ Å^{-1}. The black, red and blue solid lines, respectively, indicate $F_s^{H,G}(\kappa, t), F_s^H(\kappa, t)$ and $\widetilde{F}_s^H(\kappa, t)$ and the dashed line indicates $R(\kappa, t)$ in Eq. (5). (For interpretation of the references to color in this figure legend, the reader is referred to the web version of this article.)

Next, the self-scattering laws $S_s^X(\kappa, \omega)$ at the short and long times are examined. As found from Eqs. (13) and (14), for $t \ll t_{cls}, S_s^X(\kappa, \omega)$ approaches the expression for free gas

$$S_s^X(\kappa, \omega) = \hbar \sqrt{\frac{\beta_{eff}^X}{4\pi E_r^X}} \exp\left[-\frac{\beta_{eff}^X}{4E_r^X}\left(\hbar\omega - E_r^X\right)^2 \right] \quad (25)$$

with the effective temperature $T_{eff}^X = 1/(k_B \beta_{eff}^X)$ given by Eq. (15). Thus, the temperature dependence of $S_s^X(\kappa, \omega)$ is well characterized by T_{eff}^X. At six temperatures from 293.6 to 800 K, T_{eff}^H is calculated by use of the generalized frequency distributions in the previous study (Abe et al., 2014), and shown in Fig. 2 comparing with experimental data measured by deep inelastic neutron scattering (Uffindell et al., 2000) and ENDF/B-VII data (Chadwick, 2006). Calculated T_{eff}^H by GAAQC (open circles) and that of ENDF/B-VII (open squares) almost agrees with experimental data (full squares). The difference among
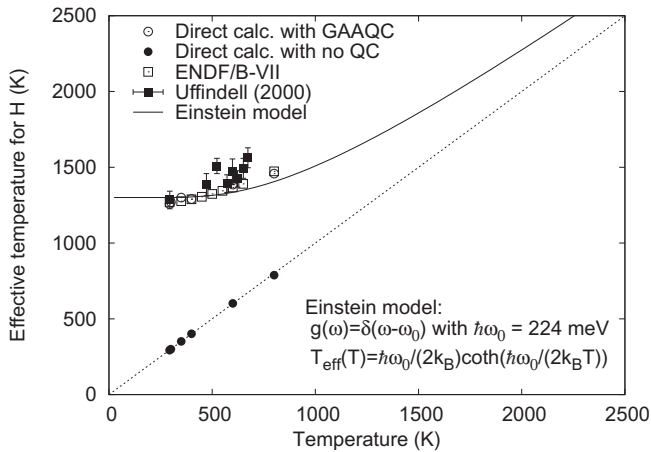
them at high temperatures may be due to the condition of the experiment, because the experimental data are measured under the constant density of 0.85 g/cm^3, which is somewhat larger than that of the MD simulation.

Moreover, the temperature dependence of T_{eff}^H is well reproduced by the Einstein model $g(\omega) = \delta(\omega - \omega_0)$ with $\hbar\omega_0 = 224$ meV, which approximately corresponds to the average energy of the frequency distribution for hydrogen (see Fig. 3). This means that the departure of T_{eff}^H from the straight line with decreasing temperature is attributed to the zero point vibration of hydrogen. This quantum effect is inherently involved in the SISF by GA because it satisfies the detailed balance condition and sum rules up to second order. Since the SISF by GAAQC approaches to the one by GA in the short time as shown in Eq. (13), it reproduces the quantum effect as well. This is the reason for a good agreement between the effective temperatures of ENDF/B-VII based on GA and that of GAAQC. On the other hand, T_{eff}^H by the direct calculation with no QC (full circles), which is evaluated as the mean kinetic energy of hydrogen atoms from MD trajectory data, has a trivial relation of $T_{eff}^H = T$ because MD simulation is essentially based on classical mechanics. By GAAQC, this classical relation is appropriately corrected as shown above.

Since, for large $t, F_s^X(\kappa, t)$ approaches $\widetilde{F}_s^X(\kappa, t)$ given by the MD simulation, $S_s^X(\kappa, \omega)$ is supposed to be dominated by QENS from the molecular diffusion. To examine the diffusive behavior of molecules from the QENS peak, calculated $S_s^H(\kappa, \omega)$ is fitted to the model by Teixeira et al. (1985), which is represented by the product of the translational and rotational diffusion components. Typical results of $S_s^H(\kappa, \omega)$ calculated at $\kappa = 1.6$ Å^{-1} and $T = 293.6$ K by GAAQC and GA are shown in Fig. 4, together with the fitted curves. As found in the figure, $S_s^H(\kappa, \omega)$ by GAAQC have a narrower QENS peak than that by GA, and both results are well reproduced by the fitting model. Thus, the half width at half maximum (HWHM) of the QENS peak for the translational diffusion component is evaluated as a function of κ^2, and shown in Fig. 5 together with experimental data (Teixeira et al., 1985). While the HWHM by GA (full circles) increasing in proportional to κ^2 corresponds to the continuous diffusion, the HWHM by GAAQC (open circles) showing more suppressed

Fig. 2. Temperature dependence of the effective temperature for hydrogen in light water. The open circles are the calculated the result by the direct calculation with GAAQC (Eq. (15)) and the full circles are the result by the direct calculation with no QC. The open and full squares indicate, respectively, ENDF/B-VII (Chadwick, 2006) and experimental data measured by deep inelastic neutron scattering (Uffindell et al., 2000). The solid line is the calculated result from Eq. (15) by the Einstein model $g(\omega) = \delta(\omega - \omega_0)$ with the single vibration energy $\hbar\omega_0 = 224$ meV. The dashed line indicates $T = T_{eff}$ for reference.
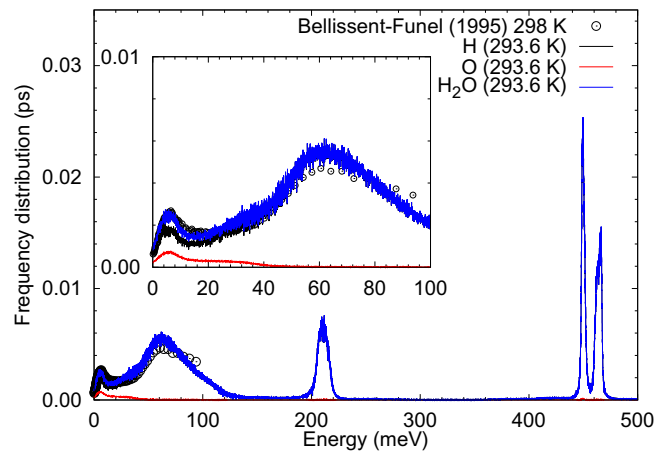

Fig. 3. Frequency distributions for hydrogen (black), oxygen (red) and water (blue) calculated at 293.6 K. The open circles indicate experimental data (Bellissent-Funel et al., 1995). Note that the magnitude of the experimental data is scaled by the height of bending peak around 6 meV because the original data are given in arbitrary unit. The enlarged spectra below 100 meV are shown in the inset. For more detailed explanation of each vibration mode, see Ref. Abe et al. (2014). (For interpretation of the references to color in this figure legend, the reader is referred to the web version of this article.)
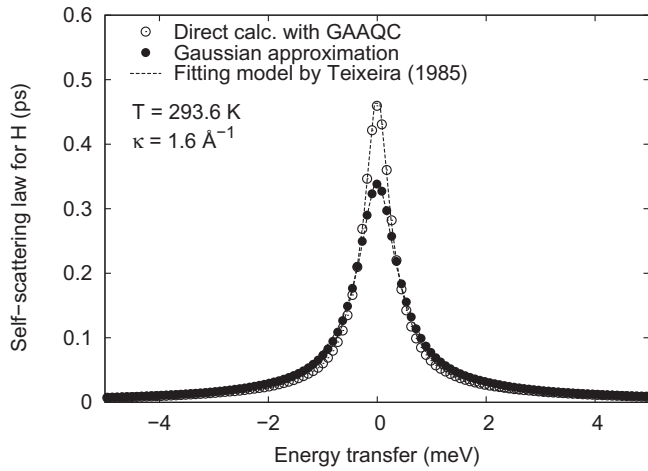
Fig. 4. Self-scattering laws for hydrogen calculated at $T = 293.6$ K and $\kappa = 1.6$ Å^{-1}. Open and full circles indicate, respectively, the results by the direct calculation with GAAQC and by GA. Dashed lines are fitted curves by the model used for analysis in Ref. Teixeira et al. (1985).

increase for $\kappa^2 > 0.5$ Å^{-2} indicates the jump-diffusion, and is in good agreement with the experiment. By fitting the HWHM by GAAQC to the jump-diffusion model $\Gamma(\kappa) = \hbar D \kappa^2 / (1 + D \kappa^2 \tau_0)$, the diffusion coefficient D and the residence time τ_0 are estimated. The estimated values of $D = 0.24$ Å^2·ps^{-1} and $\tau_0 = 1.2$ ps are also consistent with the experiment. Thus, the direct calculation with GAAQC is confirmed to reproduce the non-Gaussian behavior of the SISF for large t.

3.3. Double differential and total cross-sections

For comparison in absolute unit, the double differential scattering cross-section at 293.6 K for the incident neutron energy $E_0 = 3$ meV and the scattering angle $\theta = 71$ deg is calculated and shown in Fig. 6, together with experimental data (Novikov et al., 1999). In the figure, the positive energy transfer $\hbar\omega > 0$ means down-scattering. Note that the calculated results are convoluted with the Gaussian resolution function with $\sigma = 0.14$ meV. As the corresponding $\kappa = 1.4$ Å^{-1} at $\hbar\omega = 0$ is relatively small, QENS
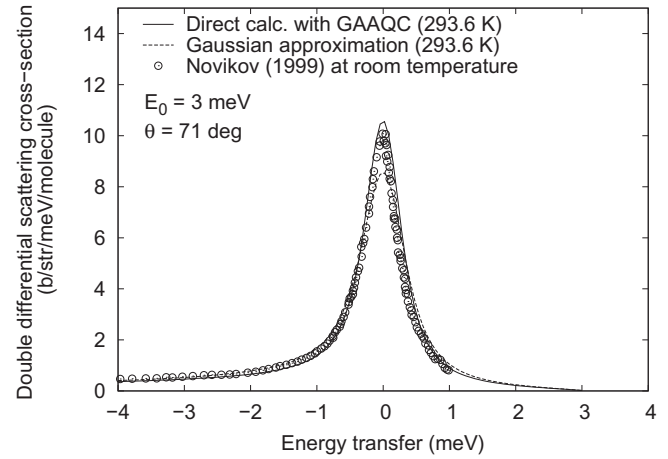

Fig. 6. Double differential scattering cross-sections of light water calculated at 293.6 K for the incident neutron energy $E_0 = 3$ meV and the scattering angle $\theta = 71$ deg. The solid and dashed lines indicate, respectively, the result by the direct calculation with GAAQC and by GA. For comparison with experimental data (open circle) (Novikov et al., 1999), the calculated results are convoluted with the Gaussian resolution function with $\sigma = 0.14$ meV.

around $\hbar\omega = 0$ is dominant. Similar to Fig. 4, the result by GAAQC (solid line) has a higher and narrower peak than that by GA (dashed line), and shows better agreement with experimental data.

To examine the overall effect of GAAQC on the scattering cross-section, total cross-sections at 293.6 and 350 K are calculated for E_0 from 1 μeV to 10 eV and shown in Fig. 7, together with the results by GA, ENDF/B-VII (Chadwick, 2006) and experimental data (Zaitsev et al., 1991; Heinloth, 1961; Russell Jr. et al., 1966). In calculating ENDF/B-VII results, the standard code, NJOY (MacFarlane and Muir, 1994) is used and the cross-section for oxygen is treated as a free gas.

While the results by GAAQC and GA are almost the same above 10 meV, the results by GAAQC are slightly smaller than that by GA below 10 meV, and in particular at 293.6 K, reproduces the experiment more closely. This can be interpreted as follows. As a result of the direct calculation of the STSCF, the translational diffusion of water molecules becomes more suppressive. This leads to a narrower QENS peak and less contribution to the total cross-section
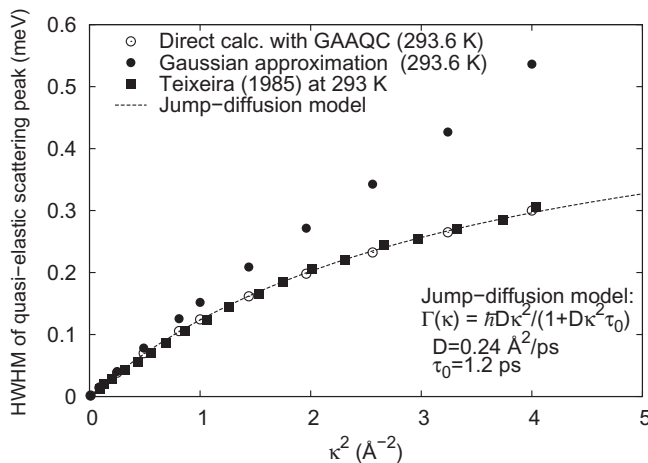

Fig. 5. The HWHM of the QENS peak for the translational component as a function of κ^2. Open and full circles indicate, respectively, the result by the direct calculation with GAAQC and by GA. Full squares are experimental data (Teixeira et al., 1985). The dashed line is a fitted curve by the jump-diffusion model and the values of estimated parameters are also shown in the figure.
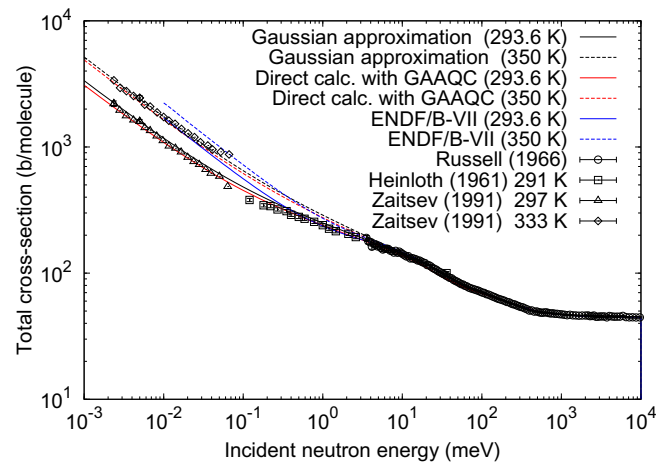

Fig. 7. Total cross-sections for light water calculated at 293.6 and 350 K. The red, black and blue lines indicate, respectively, the result by the direct calculation with GAAQC, GA and ENDF/B-VII (Chadwick, 2006). The symbols are experimental data (Zaitsev et al., 1991; Heinloth, 1961; Russell Jr. et al., 1966). (For interpretation of the references to color in this figure legend, the reader is referred to the web version of this article.)
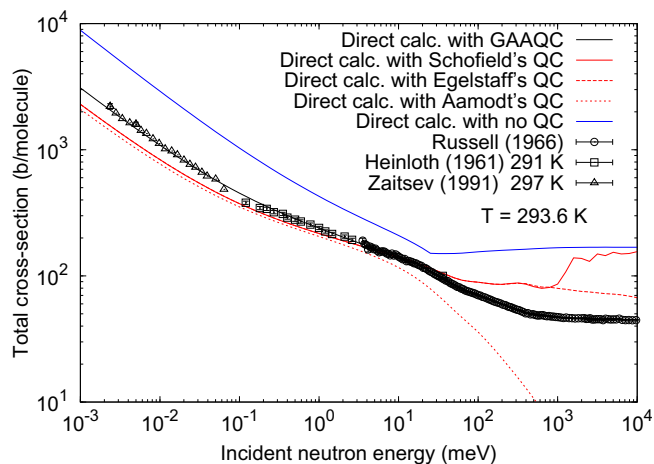
Fig. 8. Total cross-sections for light water calculated at 293.6 K. The back and blue lines are, respectively, the results with GAAQC and with no QC. Three red lines indicate, respectively, the result with the QC by Schofield (1960) (solid), Egelstaff (1962) (dashed) and Aamodt et al. (1962) (dotted). The symbols are experimental data (Zaitsev et al., 1991; Heinloth, 1961; Russell Jr. et al., 1966). (For interpretation of the references to color in this figure legend, the reader is referred to the web version of this article.)

because more restricted diffusion of molecules results in less chance to exchange their kinetic energy with incident neutrons. At 350 K, the difference between GAAQC and GA decreases since the translational diffusion tends to approach the normal diffusion. The present result indicates that the difference of the translational diffusion of water molecules can influence on the total cross-section below cold neutron energies, and hence the local difference of the molecular diffusion in water-contained materials could be detected by neutron TOF imaging if sufficient spatial resolution is achieved.

In comparison with ENDF/B-VII, the present MD-based methods (GAAQC and GA) show an advantage below cold neutron energies. Total cross-sections of ENDF/B-VII tend to overestimate experimental data below 1 meV, which would be attributed to the model used in ENDF/B-VII where the molecular translational motion is treated as a gas of molecular clusters (Mattes and Keinert, 2005).

Finally, to compare GAAQC with other QCs, total cross-sections with the QC by Schofield (1960), Egelstaff (1962) and Aamodt et al. (1962), and with no QC are calculated at 293.6 K and shown in Fig. 8, together with experimental data (Zaitsev et al., 1991; Heinloth, 1961; Russell Jr. et al., 1966). The advantage of the present method is obvious. The results by the conventional QCs deviate substantially from the free-atom cross-section of light water showing numerically strange behavior above 100 meV, which would be attributed to the failure of high-order sum rules. The result with no QC overestimates experimental data over the whole energy range, and indicates that QCs are indispensable for the evaluation of the neutron scattering cross-section from the STSCF obtained by MD simulations.

4. Concluding remarks

For the purpose of improving and generalizing the evaluation of the neutron scattering cross-section for light water, direct analysis of the STSCF from MD trajectory data is carried out, and incoherent neutron scattering cross-sections are calculated with a newly developed QC. The properties of GAAQC are as follows: (1) GAAQC is contrived from the QC by Sears in combination with the SISFs by

GA. (2) At the short time, the SISF by GAAQC approaches to the one by GA, and at the long time, to the one obtained directly from MD trajectory data. (3) The detailed balance condition and sum rules up to second order are satisfied adequately.

The effective temperature of hydrogen measured by deep inelastic scattering and the jump-diffusive behavior of the translational motion measured by QENS are well reproduced by the direct calculation with GAAQC. As comparing with GA, double differential and total cross-sections by GAAQC show better agreement with experimental data, particularly below the cold neutron region. Moreover the advantage of GAAQC is found to be apparent in comparison with other conventional QCs.

As GAAQC is quite general, it is also applicable to incoherent neutron scattering cross-sections for other materials. Thus, the present method provides the direct connection of MD trajectory data with the neutron scattering cross-section, and would serve for the detailed analysis of experimental data measured by inelastic and quasi-elastic neutron scattering, and neutron TOF imaging. Furthermore, direct analysis of coherent neutron scattering is also possible. Therefore, for advanced research, the evaluation of the neutron scattering cross-section for heavy water is now in progress and will be reported in near the future.

References

Aamodt, R., Case, K.M., Rosenbaum, M., Zweifel, P.F., 1962. Phys. Rev. 126, 1165.
Abe, Y., Tsuboi, T., Tasaki, S., 2014. Nucl. Instrum. Method A 735, 568.
Bellissent-Funel, M.-C., Chen, S.H., Zanotti, J.-M., 1995. Phys. Rev. E 51, 4558.
Biesdorf, J., Oberholzer, P., Bernauer, F., Kaestner, A., Vontobel, P., Lehmann, E.H., Schmidt, T.J., Boillat, P., 2014. Phys. Rev. Lett. 112, 248301.
Chadwick, M.B. et al., 2006. Nucl. Data Sheets 107, 2931.
Dang, L.X., Pettitt, B.M., 1987. J. Phys. Chem. 91, 3349.
Egelstaff, P.A., 1962. Adv. Phys. 11, 203.
Heinloth, K., 1961. Z. Phys. 163, 218.
Josic, L., Lehmann, E.H., Mannes, D., Kardjilov, N., Hilger, A., 2012. Nucl. Instrum. Method A 670, 68.
Kardjilov, N., Baechler, S., Bastürk, M., Dierick, M., Jolie, J., Lehmann, E., Materna, T., Schillinger, B., Vontobel, P., 2003. Nucl. Instrum. Method A 501, 536.
Kawabata, Y., Hino, M., Matsushima, U., Horie, T., Nakano, T., Maruyama, R., 2005. J. Radioanal. Nucl. Chem. 264, 319.
Kiyanagi, Y., Mizukami, K., Kamiyama, T., Hiraga, F., Iwasa, H., 2005. Nucl. Instrum. Method A 542, 316.
Kiyanagi, Y., Sato, H., Kamiyama, T., Shinohara, T., 2012. J. Phys.: Conf. Ser. 340, 012010.
MacFarlane, R.E., Muir, D.W., 1994. The NJOY Nuclear Data Processing System Version 91, LA-12740-M.
Marquez Damian, J.I., Malaspina, D.C., Granada, J.R., 2013. J. Chem. Phys. 139, 024504.
Márquez Damián, J.I., Granada, J.R., Malaspina, D.C., 2014. Ann. Nucl. Energy 65, 280.
Mattes, M., Keinert, J., 2005. Thermal Neutron Scattering Data for the Moderator Materials H$_2$O, D$_2$O and ZrH$_x$ in ENDF-6 Format and as ACE Library for MCNP(X) Codes, IAEA Report INDC(NDS)-0470.
Muhrer, G., Hartl, M., Mocko, M., Tovesson, F., Daemen, L., 2012. Nucl. Instrum. Method A 681, 91.
Novikov, A.G., Rodnikova, M.N., Savostin, V.V., Sobolev, O.V., 1999. J. Mol. Liq. 82, 83.
Rahman, A., Singwi, K.S., Sjölander, A., 1962. Phys. Rev. 126, 986.
Russell, J.L. Jr., Neill, J.M., Brown, J.R., 1966. Total Cross Section Measurements of H$_2$O, General Atomic Report GA-7581.
Schofield, P., 1960. Phys. Rev. Lett. 4, 239.
Sears, V.F., 1985. Phys. Rev. A 31, 2525.
Singwi, K.S., Sjölander, A., 1960. Phys. Rev. 119, 863.
Smith, W., Yong, C.W., Rodger, P.M., 2002. Mol. Simul. 28, 385.
Teixeira, J., Bellissent-Funel, M.-C., Chen, S.H., Dianoux, A.J., 1985. Phys. Rev. A 31, 1913.
Uffindell, C.H., Kolesnikov, A.I., Li, J-C., Mayers, J., 2000. Phys. Rev. B 62, 5492.
Van Hove, L., 1954. Phys. Rev. 95, 249.
Zaitsev, K.N., Petrov, V.N., Kuznetsov, S.P., Langer, O.A., Meshkov, I.V., Perekrestenko, A.D., 1991. Sov. At. Energy 70, 238.